Journal of Machine Engineering, 2026, Vol. 26, No. 1, 127–150
ISSN 1895-7595 (Print) ISSN 2391-8071 (Online)

Received*: 05 November 2025* /Accepted: *05 December 2025* / Published online: *24 January 2026*

3D concrete printing,
concrete additive manufacturing,
precision in 3D printing
predictive modeling,

Mouad EL MESOUDY[1*], Rida FOULKI[2],
Mouhssine CHAHBOUNI[1], Driss AMEGOUZ[1]

GEOMETRIC AND DIMENSIONAL IMPRECISIONS CLASSIFICATION AND FORM PREDICTION IN 3D CONCRETE PRINTING

3D concrete printing (3DCP) is rapidly advancing as an innovative construction method, yet achieving high dimensional and geometric accuracy remains a significant challenge. This study introduces a predictive modeling framework designed to forecast the main geometric deviations observed in 3DCP, namely planar, lateral, and vertical inaccuracies. Building on insights from 27 referenced studies, deviation sources are classified and expressed through mathematical transformation equations. The framework couples these equations with CAD-generated geometries to reconstruct the expected as-printed form before fabrication. Validation using a circular printed wall demonstrates the model's ability to predict typical distortions and quantify their magnitude, particularly those arising from slicing artefacts, material shrinkage, and interlayer deformation. By relating deviation prediction to parameter optimization, the study outlines corrective strategies such as adaptive slicing, variable-nozzle control, and targeted reinforcement. The proposed approach provides a systematic pathway for improving geometric precision and advancing 3DCP toward reliable full-scale construction.

1. INTRODUCTION

The construction industry has witnessed significant technological advancements in recent years, with 3D concrete printing (3DCP) standing out as one of the most innovative technologies [1–6]. Based on the principles of additive manufacturing (AM), 3DCP, also referred to as Additive Manufacturing of Concrete (AMoC) [3], enables the construction of complex structures layer by layer, offering numerous advantages such as material efficiency, reduced labour costs, framework need elimination, enhanced design flexibility, and accelerated project timelines [1–6]. These benefits have the potential to revolutionize traditional construction practices and address pressing challenges such as housing shortages and the demand for sustainable construction methods [1, 5].

[1]Technologies and industrial services Laboratory, EST, SMBA University, Fez, Morocco, Morocco
[2]Civil Engineering Department, ENSAM, Moulay Ismail University, Meknes, Morocco, Morocco
[*]E-mail: mouad.elmesoudy@usmba.ac.ma
https://doi.org/10.36897/jme/215220

However, as promising as 3DCP may be, achieving high levels of dimensional and geometric precision remains one of the most critical challenges [1, 3–12]. The accuracy of printed structures is a crucial factor in determining their structural integrity, functionality, and aesthetic quality. Minor deviations in geometry or dimensions can lead to significant issues, including structural instability, material waste, or the failure to meet design specifications [7–9] as shown in Fig. 1. These challenges stem from a combination of factors, including the rheological behaviour of cementitious materials, the dynamic nature of printing parameters, and external environmental influences such as temperature and humidity [7–11]. Additionally, the inherent complexity of the 3D Printing (3DP) process, involving precise material deposition and the interaction of multiple mechanical and software systems, further compounds these difficulties [10–12].

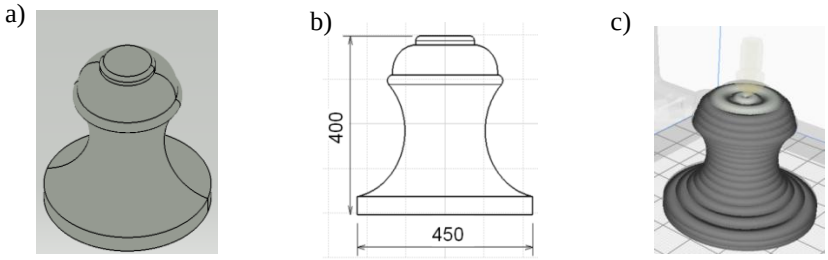

Fig.1. The geometrical and dimensional gaps in 3DCP, (a) the CAD view of the structure in CATIA V5 (450 mm in base diameter and 400 mm in height), (b) the dimensions of the model, and (c) the simulation of the 3D printed structure in UltimakerCura using a 60×20 mm layer width and height

This article aims to classify and analyse the main sources of geometric and dimensional imprecision in 3DCP based on a systematic review of existing works and then proposes a predictive framework using the imprecisions parameters and sources to estimate deviations and forecast the final printed geometry.

Section 2 presents a review of the historical development and current techniques of 3DCP. Section 3 explains the research methodology, including the review of more than 25 publications and the classification approach. Section 4 introduces the deviation taxonomy, distinguishing between planar, lateral, and vertical imprecisions. Section 5 describes the predictive modeling method and provides an experimental validation through a circular-wall printing test. Section 6 discusses the implications of the findings and the main challenges to achieving high-precision 3DCP. Finally, Section 7 summarizes the conclusions and outlines perspectives for future research.

2. LITERATURE REVIEW

2.1. HISTORICAL DEVELOPMENT OF 3DCP

The origins of automation in concrete construction can be tracked to the beginning of the 20th century when new techniques such as slip forming [1] and shotcreting [13] were firstly introduced. Moving to the mid 1980s, when a new AM or 3DP emerged [1, 2]. The ASTM International Committee F42 defines AM as the process of joining materials to

make objects from 3D model data, usually layer upon layer [14]. AM started gaining interest in industries like biomedical, aerospace and automotive manufacturing and probably this is when people started thinking of a way to integrate this new emerging technology into the concrete construction field [1].

Few years later, specifically, in the mid-1990's, the first attempt of combining 3DP and concrete was introduced by Khoshnevis who innovated “Contour Crafting”, a technology based on extruding the material and deposing it as continuous filament layer by layer without the need of formworks [1–4]. Another technology, currently termed as “D-Shape” [1–4], consisting on selectively deposing a binder (cement for example) on a sand matrix to join the grains was developed at the same time in the mid-1990s [3]. Moving to the beginning of the 21st century when an alternative technology noted as “Freeform Construction” or “Concrete Printing” surfaced allowing printing with smaller resolutions for greater precision and finer details [1, 4]. Since then, the development of 3DCP has been steady, until 2012, when people start realizing the real potential of this impressive process of construction which made the number of researches and experimental works multiplies and the rate of developments going much faster [3].

2.2. TECHNIQUES USED IN 3DCP AND PRINTING PARAMETERS

3DCP consists on conveying concrete using a pump towards a printer head fixed on gantry system or a robotic arm and moving on a predefined trajectory to create the desired shape [1-5]. The pump can be replaced by a tank mounted on or near the printer head, allowing the concrete to be extruded either through a piston-driven system or a screw-based mechanism [5, 15, 16]. As previously mentioned, there are two main types of 3DCP techniques. The first is extrusion-based printing, such as Contour Crafting and Concrete Printing, where concrete is deposited layer by layer to build the desired structure [1–5]. The second is powder-based printing, with D-Shape as a representative example [2, 9, 17]. In this approach, concrete particles are selectively connected using specific binders to form the final product [2, 9, 17].

Another critical aspect of 3DCP involves the printing parameters, which can generally be categorized into three groups: printer parameters, material parameters, and printed structure parameters [1–6, 15–20]. The material parameters usually refer to the concrete rheological properties, including printability, buildability, and extrudability [1–6, 16–18]. Under printer parameters, key factors include the printing speed characterizing the nozzle movement, the concrete’s extrusion rate flow and the nozzle size which directly affect the printed layers form and dimensions and ultimately the final product’s resolution [1–6, 15–18] as shown in Fig. 2.

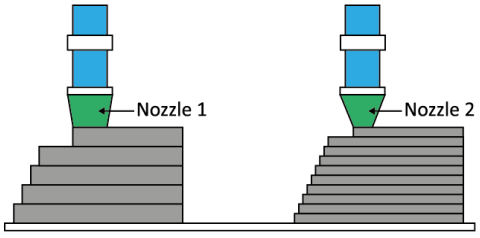

Fig.1.The nozzle size effect on the printed structure resolution

The printed structure parameters integrate generally the geometrical and dimensional characteristics, as well as the required mechanical, acoustic and thermal properties of the structure [1–6, 18–20].

3. METHODOLOGY

3.1. RELATED WORKS

Several studies have investigated approaches for quantifying and controlling geometric imprecisions in 3DCP, providing essential foundations for deviation modeling and precision assessment. Xu, J. [7] applied Geometric Dimensioning and Tolerancing (GD&T) principles to evaluate process capability, introducing key metrics such as maximum positive and negative deviation errors and mean volumetric deviations per unit area. These indicators were validated through point-cloud analyses of 3D-scanned printed elements.

Nair, S. A. [8] proposed a two-level geometric qualification framework combining visual point-cloud comparisons with a Print Accuracy Index derived from centroidal distance analysis and set-theory-based surface matching, offering a practical tool for rapid quality control. For powder-based systems, Liu, X. [9] demonstrated how fly ash can enhance mechanical performance and dimensional accuracy, emphasizing the strong link between material formulations and printing precision.

In terms of monitoring strategies, Silva, J. M. [10] developed a real-time inspection pipeline integrating depth sensing, computer vision, and machine learning (XGBoost) to adjust printing parameters dynamically during fabrication. A comprehensive review by Mawas, K. [11] further highlighted the wide range of sensing technologies—across both extrusion and shotcrete-based systems—used for geometric and surface inspection, underscoring their importance in automated deviation detection and precision assurance.

3.2 SYSTEMATIC REVIEW

A systematic review of over 27 peer-reviewed scientific publications was conducted to consolidate knowledge on different types and forms of geometrical and dimensional imprecision in 3DCP. For the selection process, publications were filtered by title, abstract, and keywords relevant to geometric deviations, printing accuracy, dimensional control and 3DCP precision. A second-level screening based on full-text content ensured the methodological relevance of each source. Furthermore, to ensure updated analysis, only works published in or after 2020 were considered. The synthesis of this literature laid the groundwork for defining our own methodology for deviation quantification and mapping, as detailed in the following section.

3.3. IMPRECISIONS AND DEVIATIONS QUANTIFICATION AND MAPPING

Based on the reviewed literature and collected data, a methodology was developed to quantify and map dimensional and geometric imprecisions in 3DCP. The approach involves

segmenting the printed structure into analysis blocks to localize deviations and better understand their causes and distribution.

Two main categories of imprecision were identified. The first one includes planar deviations that occur along the printed layers due to material properties (e.g., rheology), printer accuracy, and process parameters such as extrusion rate and speed. These lead to misalignment and irregular thickness in layers. The second category includes lateral and vertical deviations, often resulting from resolution limits, buildability issues, and structural deformations, impacting the overall dimensions and geometry of the printed object.

4. RESULTS: CLASSIFICATION OF GEOMETRIC AND DIMENSIONAL IMPRECISIONS

This section explores the various types of geometric and dimensional deviations observed in 3DCP, beginning with plane deviations along the x and y axes as illustrated in Fig. 3, and extending to lateral surface irregularities and height-based gaps.

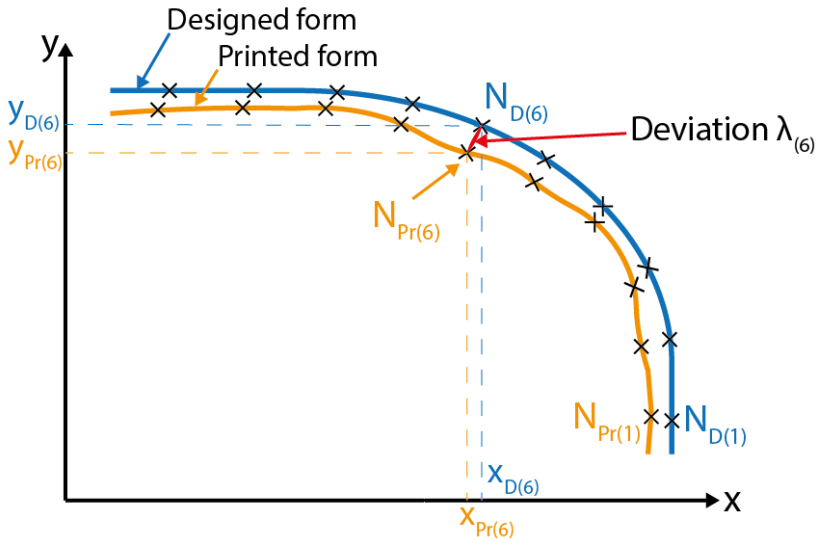

Fig.3 A schematic representation of the planar deviations

Table. 1 resumes the main metrics and their symbols used on the transformation equations mentioned on this section.

Table 1. Table of metrics symbols and physical meaning

Metrics physical meaning	Metrics symbol
Radius of the original circle	$\boldsymbol{R}$
Structure's CAD model height	$\boldsymbol{H_t}$
Printed layers height	$\boldsymbol{h_{printed}}$
Width of the target part in the cad model	$\boldsymbol{W_t}$
Initial width of the printed layer	$\boldsymbol{W_{printed}}$

* Units: All the used metrics are in mm

4.1. PLANE DEVIATIONS AND GAPS

4.1.1. MESH OR STL CONVERSION DEVIATION $\lambda_{(x,y),1}$

In 3D printing workflows, including 3DCP, the generation of toolpath begins with a CAD model that is exported to an STL format [21–23]. This conversion replaces the model's continuous surfaces with a triangulated mesh, introducing geometric approximations. As highlighted by Montalti A. [22], three main errors arise from tessellation: chord deviation, angle deviation, and maximum facet size. For curved geometries, chord deviations are the most significant, as the polygonal approximation cannot perfectly match the original curve. To illustrate chordal deviation resulting from STL conversion, we consider the case of a circle with radius *R*, which, after triangulation or tessellation, is represented by a polygon with *n* vertices. This approximation leads to measurable discrepancies between the ideal and tessellated geometries as depicted in Fig. 4.

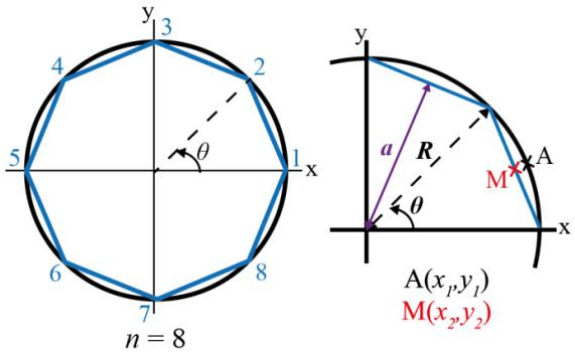

Fig.4. An example of circular and polygon model with *n*=8

The maximum deviation can be expressed mathematically as shown in Eq. (1).

$$\lambda_{(x,y),1max} = R - a = R\left(1 - \cos\left(\frac{\theta}{2}\right)\right) \text{with } \theta = \frac{2\pi}{n} \tag{1}$$

Here,n represents the number of mesh points, θ the angle of tessellation and$a$, the created polygon apothem. From Eq. (1), we observe that increasing $n$reduces $\lambda_{(x,y),1}$ exponentially, since smaller polygon segments better follow the true curvature. The function that describes the variation of the local deviation $\lambda_{(x,y),1}$ based on the angular orientation φ is given by Eq. (2) capturing how the deviation changes with the position on the arc, depending on the tessellation step and the mesh resolution.

$$\lambda_{(x,y),1} = f(\varphi) = R\left(1 - \cos\left(\varphi - \left(E\left(\frac{\varphi}{\theta}\right) \times \theta\right)\right)\right) \tag{2}$$

Although 3DCP follows a similar workflow to traditional 3DP processes, the impact of STL induced errors is generally much smaller. This is because printed structures in 3DCP are large, and modern software allows high mesh resolutions, resulting in very small facetsizes.

Consequently, STL deviations do exist but are often geometrically negligible compared with the overall dimensions of the printed object.

4.1.2.LATERAL SURFACE CONVERSION DEVIATION $\lambda_{(x,y),2}$

During the transition from a CAD model to a printable format in 3DCP, the slicing process converts complex geometries such as curves and spherical surfaces into a series of discrete horizontal layers [7, 21, 24]. This simplification can lead to a geometric deviation commonly referred to as the staircase effect [7] which becomes clearly noticeable on sloped or curved surfaces as represented in Fig. 5.

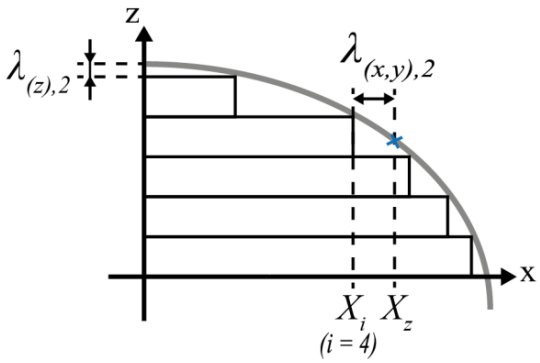

Fig.5. Deviations generated due to the vertical slicing process

Based on the schematic in Fig. 5, the deviation related to lateral surface slicing can be quantified by Eq. (3), where the deviation value depends on the vertical *z*-position of the studied point. This *z*-position determines both X_z, the x-coordinate of the original point on the CAD model, and X_i, the x-coordinate on the corresponding printed layer at height z.

$$\lambda_{(x,y),2} = f(z) = X_z - X_i \text{with } i = g(z)\ ,\ 1 \le i \le m \text{ and } m = E\left(\frac{H_t}{h_{printed}}\right) \tag{3}$$

With i the layer index corresponding to the height coordinate on z axis and m the final layer index. $\lambda_{(x,y),2}$ depends directly on the layer height, conversely, when smaller layer heights are used, the lateral conversion deviation becomes significantly reduced and may be negligible for many architectural-scale elements**.**

4.1.3.SHRINKAGE GAP (CONCRETE SETTING) $\lambda_{(x,y),3}$

Depending on the concrete composition and environmental conditions, a physical phenomenon known as shrinkage occurs during setting and dehydration, reducing the volume of the printed material. In 3DCP, four types of shrinkage can contribute to dimensional changes: drying shrinkage [25], plastic shrinkage [26], endogenous shrinkage [27], and thermal shrinkage [28]. The deviation induced by shrinkage is represented in Eq. (4) as the overall shrinkage is the cumulative effect of the four shrinkage types.

$$\lambda_{(x,y),3} = \frac{W_{printed} - W_{set}}{2} = \sum_{k=1}^{4} \lambda_{(x,y),3,k} \tag{4}$$

W_{set} is the final width after shrinkage and solidification.

Zhu L. [29] reviewed the tests used to characterize various shrinkage types, comparing the performance and influencing factors between traditional cast cement materials and those used in 3DCP. The study analysed shrinkage behaviour based on the printing process, material formulation, and curing system. Similarly, Rahul A. [30] investigated free shrinkage in printable concrete using 40 × 40 × 160 mm prism molds, following ASTM C596-01 under both drying and autogenous conditions. Federowicz K. [31] proposed an original method to measure shrinkage-induced deformations in printed elements and examined the influence of internal and external curing on the progression and final extent of shrinkage.

Despite being unavoidable, shrinkage has a minimal impact on geometric accuracy in 3DCP. Typical shrinkage strains (ε_{sh}) for concrete are extremely small, meaning that the resulting dimensional deviations are usually negligible compared to the overall scale of printed structural elements.

4.1.4. LAYER COMPRESSION DEVIATION $\lambda_{(x,y),4}$

When concrete layers are printed, the lower layers experience compressive stresses resulting from their own weight, the load of the upper layers, and the pressure exerted by the nozzle during deposition [1, 5, 32–34]. Figure 6 illustrates the deformation related to these combined stresses, causing an increase in layer width and a reduction in height.

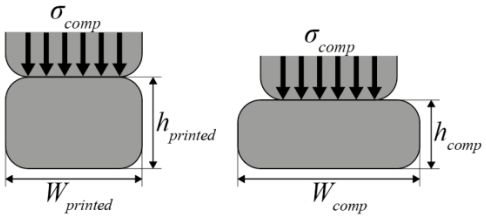

Fig.6. Deformation of the printed concrete layer under compressive stress (σ_{comp})

The planar deviation associated to this phenomenon is written as follows in Eq. (5).

$$\lambda_{(x,y),4} = \frac{W_{printed} - W_{comp}}{2} \tag{5}$$

W_{comp}represents the printed layer width after compression. Since $W_{printed} < W_{comp}$ the layer compression deviation value is negative.

Jayathilakage R. [32], tried to identify the buildability criteria based on the green strength of concrete and the effect of early age material properties on the stability of printed structures. Additionally, Liu Z. [33] investigated the fresh-state cementitious materials properties and Khan S.A. [34] elaborated an experimental and numerical study to analyse the buildability in 3DCP.

4.1.5. NOZZLE EXTRUSION SIZE EFFECT $\lambda_{(X,Y),5}$

In 3DCP, printing parameters; particularly nozzle design, size, and shape; significantly influence the final geometry of the printed layers. The nozzle outlet form and its distance from the printing surface directly affect both the width and height of the deposited concrete layers [35–37]. The relationship between nozzle characteristics and CAD dimensions can lead to a dimensional gap between the designed model and the actual printed form. Eq. (6) expresses this deviation.

$$\lambda_{(x,y),5} = W_t - W_{printed} \times E\left(\frac{W_T}{W_{printed}}\right) \tag{6}$$

In cases where $W_t < W_{printed}$, the negative gap value is modeled in Eq. (7).

$$\lambda_{(x,y),5} = W_t - W_{printed} \tag{7}$$

This issue can be addressed using technical solutions such as interchangeable nozzles or automated variable-size nozzles [36, 38].

4.1.6. ELLIPTICAL DEVIATION $\lambda_{(x,y),6}$

In 3DP processes, to generate circular, elliptical, or curved trajectories, the printer executes coordinated movements along multiple axes—most notably the x and y axes—in simultaneous harmonic motions [39]. This motion can result in a specific type of geometric deviation known as eccentricity, denoted by e, which quantifies the shape deviation between the printed contour and a perfect circle [40, 41]. In such cases, Eq. (8) is used to calculate the eccentricity.

$$e = \sqrt{1 - \frac{b^2}{B^2}} \tag{8}$$

Where B and b are respectively the semi-major and semi-minor axes of the resulting ellipse as represented in Fig. 7.

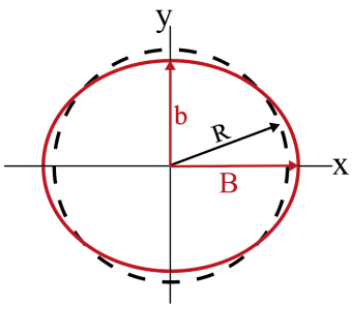

Fig.7. Elliptical deviations and eccentricity faults

When $e = 0$, the print trajectory describes a perfect circle defined by R, but for $0 < e < 1$ the trajectory is elliptical. In this case, $\lambda_{(x,y),6}$ vary between two positive and negative values (Eq. (9)).

$$b - R \leq \lambda_{(x,y),6} \leq B - R \tag{9}$$

In practice, modern 3DCP systems exhibit highly precise multi-axis synchronization**,** making eccentricity-induced deviations extremely small and generally negligible in most printed circular geometries.

4.1.7. MACHINE (PRINTER) ACCURACY DEVIATION $\lambda_{(x,y),7}$

This type of deviation is generally related to the precision of the 3DCP machine itself. These errors are quite small, usually just a few millimetres or even less, when using high-end printers and result from minor inaccuracies in axis motion, component alignment, and kinematic interactions during deposition [39]. As highlighted by Munteanu [39], modeling and compensating these mechanical imperfections within the control system remains a key challenge for enhancing geometric fidelity.

In commercial systems, this deviation can be estimated from manufacturer specifications. However, for custom-built or prototype printers, the deviation depends strongly on component characteristics, including servomotor resolution, calibration of motion controllers, and the precision of the transmission mechanisms. Overall, while generally small, machine accuracy deviation must be accounted for when predicting the final printed geometry.

4.1.8. EXTRUSION SYSTEM ACCURACY DEVIATION $\lambda_{(x,y),8}$

The extrusion system ensures the continuous supply of concrete and plays a critical role in achieving precise and uniform layers whether the system relies on rotating mechanisms or pressure-driven setups like rams [5]. As the material moves from the storage unit toward the nozzle, the transport mechanism and nozzle design can introduce flow instabilities and pressure losses, which reduce extrusion efficiency and lead to narrower printed layers [35, 42, 43]. Maroszek M. [42] investigated factors affecting extrusion performance, including how material flow rates respond to different input parameters. Yuan P.F. [43] proposed a variable-width 3DCP system through controlled extrusion.

4.2. LATERAL SURFACE AND VERTICAL (HEIGHT) DEVIATIONS

While planar deviations primarily concern errors along the x–y plane, 3DCP also exhibits notable irregularities along the lateral surfaces and the vertical (z-axis) dimension, as discussed in the following section.

4.2.1. INTERLAYER NOTCH OR STAIRCASE EFFECT ON LATERAL SURFACE

The layer-by-layer process used in 3DCP often produces a lateral surface with bulging shapes, commonly referred to as interlayer notches [44] or the staircase effect [7]. When the individual layers are too visible, they create a rough and visually unappealing surface finish as illustrated in Fig. 8.

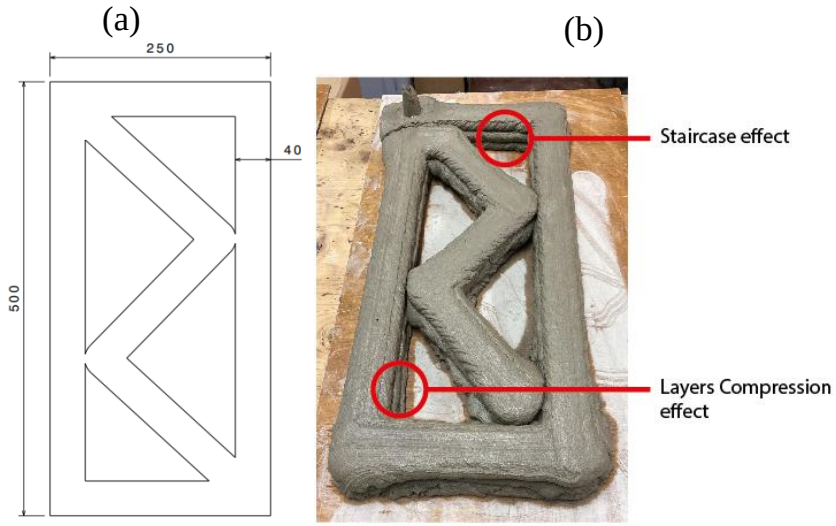

Fig.8. (a) The sample CAD model front view with dimensions and (b) 3 printed layers of the sample showing the "staircase effect" on lateral surface in 3DCP and visualizing the layers compression effect on inferior printed layers

This issue is mainly caused by printing parameters particularly the characteristics of the nozzle, which directly influence the printing resolution as shown is Fig. 2.

4.2.2. SHRINKAGE GAP $\lambda_{(z),1}$

Shrinkage in height follows the same principles described in Section 4.1 for planar shrinkage ($\lambda_{(x,y),3}$), but here, it impacts the vertical dimension [25–31]. This deviation is represented in Eq. (10) withh_{set}, the printed layers height after setting and solidification.

$$\lambda_{(z),1} = \frac{h_{printed} - h_{set}}{2} = \sum_{k=1}^{4} \lambda_{(z),1k} \tag{10}$$

4.2.3 LAYER COMPRESSION HEIGHT DEVIATION $\lambda_{(z),2}$

The compressive stresses applied on the printed layers create deviation on the layers height [1, 5, 32–34] as depicted in Fig. 6. The height deviation is calculated as follows in Eq. (11).

$$\lambda_{(z),2} = \frac{h_{printed} - h_{comp}}{2} \tag{11}$$

h_{comp} is the layers height after compression.

4.2.4. MACHINE PRECISION DEVIATION $\lambda_{(z),3}$

The printing system can also introduce vertical deviations stemming from the accuracy of the movement mechanism along the z-axis, which is directly influenced by the printer's kinematics and overall mechanical precision [39].

4.2.5. SLICING DEVIATION $\lambda_{(z),4}$

The horizontal slicing process generates another form of deviation when using nozzles with large extrusion outlets or low-resolution settings, which can affect the vertical accuracy of the printed layers [21, 24].

In such cases, a *z*-axis deviation may occur at the top of the structure, where the final part is not printed because the layer height ($h_{printed}$) exceeds the remaining height of the model (see Fig. 2 and Fig. 5). This vertical deviation can be calculated using Eq. (12).

$$\lambda_{(z),4} = H_t - h_{printed} \times E\left(\frac{H_t}{h_{printed}}\right) \tag{12}$$

4.3 RESULTS SUMMARY

The actual dimensions and geometrical aspects of the printed structure can be predicted by calculating the sum of the deviations resulting either from the printing process, the cementitious material used, or the machine employed.

For the *x*-coordinates, as Eq. 13 represents, the sum of planar deviations is used by projecting each deviation on the *x*-axis using the angle of inclination α_j ($j\epsilon[1,n]$ with n the number of points) which defines the studied point's orientation in the (x, y) plane.

$$\begin{bmatrix} x_{P1} \\ \vdots \\ x_{Pn} \end{bmatrix} = \begin{bmatrix} x_{N1} \\ \vdots \\ x_{Nn} \end{bmatrix} - \begin{bmatrix} \sum_{i=1}^{8} (\lambda_{(x,y),i,N1} \times \cos(\alpha_1)) \\ \vdots \\ \sum_{i=1}^{8} (\lambda_{(x,y),i,Nn} \times \cos(\alpha_n)) \end{bmatrix} \tag{13}$$

Hence $x_{Pj} = x_{Nj} - \sum_{i=1}^{8} (\lambda_{(x,y),i,Nj} \times \cos(\alpha_j))$ with $1 \leq j \leq n$

For the *y*-axis, the same application is used, projecting the deviations onto the *y*-axis as shown in Eq. (14).

$$\begin{bmatrix} y_{P1} \\ \vdots \\ y_{Pn} \end{bmatrix} = \begin{bmatrix} y_{N1} \\ \vdots \\ y_{Nn} \end{bmatrix} - \begin{bmatrix} \sum_{i=1}^{8} (\lambda_{(x,y),i,N1} \times \sin(\alpha_1)) \\ \vdots \\ \sum_{i=1}^{8} (\lambda_{(x,y),i,Nn} \times \sin(\alpha_n)) \end{bmatrix} \tag{14}$$

Hence $y_{Pj} = y_{Nj} - \sum_{i=1}^{8} (\lambda_{(x,y),i,Nj} \times \sin(\alpha_j))$ with $1 \leq j \leq n$

For *z*, the height deviations related to shrinkage, compression and printer precision are summed to obtain the vertical deviation for each layer, as expressed in Eq. (15).

$$\begin{bmatrix} z_{P1} \\ \vdots \\ z_{Pn} \end{bmatrix} = \begin{bmatrix} z_{N1} \\ \vdots \\ z_{Nn} \end{bmatrix} - \begin{bmatrix} \lambda_{(z),1,N1} + \lambda_{(z),2,N1} + \lambda_{(z),3,N1} \\ \vdots \\ \lambda_{(z),1,Nn} + \lambda_{(z),2,Nn} + \lambda_{(z),3,Nn} \end{bmatrix} \tag{15}$$

Hence $z_{Pj} = z_{Nj} - \lambda_{(z),1,Nj} + \lambda_{(z),2,Nj} + \lambda_{(z),3,Nj}$ with $1 \leq j \leq n$

The deviation associated with the slicing process $\lambda_{(z),4}$ is only added to the other deviations for the points belonging to the higher section of the printed product that has not been printed due to the nozzle resolution as depicted in Fig. 7.

5.PREDICTIVE MODELING APPROACH IN 3DCP

5.1. OVERVIEW

The predictive modeling framework proposed in this study begins with the virtual geometry of the target structure, where the coordinates of every point are extracted from the CAD model. Next, the printing and deviation factors—derived from the classification scheme presented earlier—are defined to represent the main sources of dimensional inaccuracy. These parameters feed into the mathematical core of the framework, which uses the equations and transformation matrices developed to compute the expected displacements at each point. The results are then assembled to reconstruct the predicted as-printed geometry, enabling direct comparison with the original design and facilitating proactive compensation strategies.

5.2. INPUT PARAMETER DEFINITION AND CLASSIFICATION

Based on the classification of geometric and dimensional deviations presented in the previous section, each form of imprecision is associated with one or more influencing

parameters these parameters serve as the predictive modeling algorithm's primary inputs, allowing for precise mathematical computation of the finished printed form. These parameters definition and registration are essential to the simulation process since they enable the framework toidentify deviation sources andquantify the magnitude of each parameter's impact on the final geometry.

To ensure accurate prediction, the main parameters to be input and implemented in the model are grouped into 4 categories as represented in Table 2.

Table 2 Input parameters categories

Category	Input parameters
Material-related parameters	Rheology (yield stress, viscosity) Shrinkage strain coefficient
Process-related parameters	Printing speed Layer height Extrusion rate Nozzle path accuracy The meshing or STL conversion resolution
Environmental parameters	Temperature Humidity Wind/airflow conditions
Machine-related parameters	Nozzle diameter Positioning precision (x, y, z axes) Vibrations or mechanical instability

These parameters are systematically recorded and used as direct inputs in the mathematical calculation stage of the predictive approach. Each parameter is assigned to its corresponding deviation category from the classification section, creating a structured mapping between deviation types and influencing factor.

5.3.COMPUTATION AND CALCULATION

The predictive model computes the as-printed geometry by integrating the virtual CAD or STL derived coordinates with the influence of quantified deviation sources. Using as inputs the sliced virtual form, the full parameter set (material, process, environmental, and machine-related variables defined in Section 5.2), and the established deviation models, the algorithm applies the mathematical functions and matrix operations described in Equations (13-15) to project and accumulate deviations on the *x*, *y*, and z axes. The computation proceeds iteratively for every studied point, layer by layer, summing the contribution of each deviation source to reconstruct the evolving geometry of the printed element. The final outputs consist of the predicted coordinates of all points in the printed layers ($x_{\mathrm{P}\,(i)}$, $y_{\mathrm{P}\,(i)}$, $z_{\mathrm{P}\,(i)}$) and a complete 3D point cloud or mesh representing the expected as-printed geometry.

To implement the computation, various software environments can be used depending on complexity and integration needs. MATLAB is particularly suited for advanced numerical computation, matrix manipulation, and 3D visualization, making it ideal for implementing the transformation equations and performing parameter sensitivity studies. Python, as an

open-source and highly flexible environment, excels in data processing and is well adapted for developing custom predictive scripts or integrating deviation models with point-cloud or scanning data. For rapid, on-site estimations, Excel or LibreOffice Calc provides an accessible solution for handling small-scale models or generating quick deviation calculations. CAD-oriented tools such as ANSYS SpaceClaim or SolidWorks allow deviation transformations to be applied directly to digital geometries, facilitating visual inspection of predicted shapes. Finally, cloud-based BIM platforms, including Autodesk BIM 360, support collaborative workflows, version control, and centralized data management, enabling construction teams to integrate predicted geometries within broader project coordination processes.

5.4. OUTPUTANALYSIS

Once the predicted form is generated, its dimensional accuracy and geometric precision are evaluated by directly comparing it to the original virtual model. This comparison involves calculating point-to-point deviations and visualizing them through deviation maps, which highlight both the magnitude and spatial distribution of errors across the structure. Such maps enable the identification of critical zones that may require process adjustments, including areas affected by over- or under-extrusion, layer misalignment, or localized deformation.

Statistical metrics like the Mean Absolute Deviation (MAD), Root Mean Square Error (RMSE), and maximum deviation values are calculated to give quantitative measurements of prediction accuracy in addition to visual assessment. Within the predictive framework, the related input parameters, such as printing speed, extrusion rate, layer height, or material rheology, may be changed repeatedly if the deviation levels above acceptable tolerances. By enabling parameter improvement, this feedback approach guarantees increased accuracy in successive forecasts and real prints (see Fig. 9).

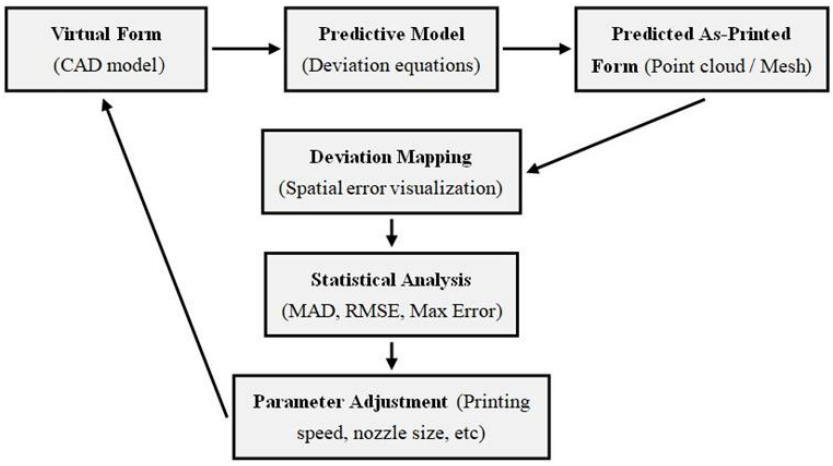

Fig.9. Flow diagram showing the cycle from virtual form to parameter adjustment

5.5.EXPERIMENTAL TEST AND VALIDATION

To evaluate the reliability of the proposed deviation-based approach, an experimental test was conducted using a circular wall printed under controlled conditions. The objective of

this validation step is to compare the CAD designed model**,** the predicted geometry**,** and the printed form to analyse the model's capability to predict real deviations in 3DCP.

5.5.1.TEST GEOMETRY, PRINTING SETUP AND PARAMETERS

A circular wall was selected for test due to its geometric sensitivity to both planar and vertical deviations. The design specifications are defined with a 200 mm nominal diameter (D), a wall height (H_t) of 62 mm and a width (W_t) of 45 mm. rectangular profile around a central axis located at a radial distance (d) of 100 mm from the origin, as illustrated in Fig. 10.

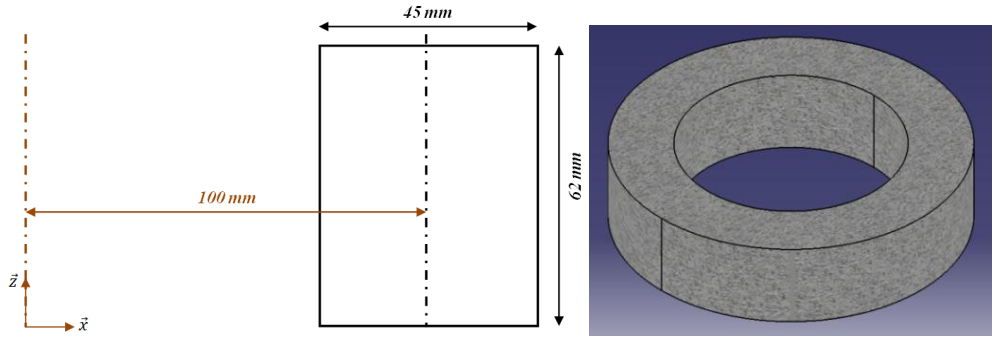

Fig.10. Geometrical specifications of the rectangular profile and the generated CAD model represented on CATIA V5

The concrete mixture consisted of Portland cement (CEM I 45), silica sand, grey silica fume, set accelerator and polypropylene fibres. For this formulation the concrete shrinkage strain (ε_{sh}) was estimated for 0.0005.

For the experimental setup, a 10 mm nozzle was mounted on a gantry-based 3DCP system with a positioning precision of 0.0001 mm. The printing speed was fixed at 75 mm/s, and the material flow rate was maintained at approximately 4 L/min. Under these operating conditions, the resulting printed layer exhibited a height ($h_{printed}$) of 20 mm and an initial width ($W_{printed}$) of 45 mm. The average time required to print a single layer is approximately 9 s.

5.5.2DEVIATION COMPUTATION AND PREDICTED GEOMETRY

Since the studied geometry results from the revolution of a rectangular profile, the printed wall consists of three identical layers, each with a height of 20 mm. For deviation computation, three representative points were selected per layer. Vertical deviations were evaluated at the uppermost point located at the mid-thickness of each layer, corresponding to$z_1 = 20$, $z_2 = 40$ and$z_3 = 60$. Planar deviations were assessed by selecting two points per layer: one on the inner surface and one on the outer surface, as illustrated in Fig. 11.Since$a_j = 0$ in this specific geometry, only deviations along the *x*-axis and the *z*-axis were considered in the computation.

Table 3 summarizes the calculated deviations for all three layers based on the proposed classification framework.

Table 3. Calculated deviations

Planar deviations (**)		
Mesh or STL conversion deviation $\boldsymbol{\lambda_{(x,y),1}}$	Since the applied STL resolution is high: $\boldsymbol{\lambda_{(x,y),1} = 0}$	
Lateral surface conversion deviation $\boldsymbol{\lambda_{(x,y),2}}$	Since $\boldsymbol{W_t}$ is constant with $\boldsymbol{z}$: $\boldsymbol{X_i - X_z}$ so$\boldsymbol{\lambda_{(x,y),2} = 0}$	
Shrinkage gap (concrete setting) $\boldsymbol{\lambda_{(x,y),3}}$	$\boldsymbol{\lambda_{(x,y),3} = \frac{\varepsilon_{sh} \times W_{printed}}{2} = \frac{0.005 \times 45}{2} = 0.1125}$	
Layer compression deviation $\boldsymbol{\lambda_{(x,y),4}}$ (***)	Layer 1: The first layer is subjected to the compression of its own weight and the weight of the two superior layers. $\boldsymbol{\lambda_{(x,y),4,1} = -2.5}$	
	Layer 2: The second layer is subjected to the compression of its own weight and the weight of the superior layer. $\boldsymbol{\lambda_{(x,y),4,2} = -1.5}$	
	Layer 3: The third layer is subjected to its own weight compression. $\boldsymbol{\lambda_{(x,y),4,3} = -0.25}$	
Nozzle extrusion size effect $\boldsymbol{\lambda_{(x,y),5}}$	Since $\boldsymbol{W_t = W_{printed}}$: $\boldsymbol{\lambda_{(x,y),5} = 0}$	
Elliptical deviation $\boldsymbol{\lambda_{(x,y),6}}$	$\boldsymbol{\lambda_{(x,y),6} = 0}$	
Machine (printer) accuracy deviation $\boldsymbol{\lambda_{(x,y),7}}$	$\boldsymbol{\lambda_{(x,y),7} = \pm(100 \times 0.0001) = \pm 0.01}$	
Extrusion system accuracy deviation $\boldsymbol{\lambda_{(x,y),8}}$	$\boldsymbol{\lambda_{(x,y),8} = 0}$	
Layer 1 planar deviations on x axis	$\boldsymbol{\lambda_{(x,y),N1,1} = -2.3875}$	$\boldsymbol{\lambda_{(x,y),N1,2} = -2.3875}$
Layer 2 planar deviations on x axis	$\boldsymbol{\lambda_{(x,y),N2,1} = -1.3875}$	$\boldsymbol{\lambda_{(x,y),N2,2} = -1.3875}$
Layer 3 planar deviations on x axis	$\boldsymbol{\lambda_{(x,y),N3,1} = -0.1375}$	$\boldsymbol{\lambda_{(x,y),N3,2} = -0.1375}$
Lateral deviations (**)		
Interlayer notch or staircase effect on lateral surface	$\boldsymbol{r = 5}$	
Vertical (height) deviations (**)		
Shrinkage gap $\boldsymbol{\lambda_{(z),1}}$	$\boldsymbol{\lambda_{(z),1} = \frac{\varepsilon \times h_{printed}}{2} = \frac{0.005 \times 20}{2} = 0.05}$	
Layer compression height deviation $\boldsymbol{\lambda_{(z),2}}$ (***)	Layer 1, $\boldsymbol{\lambda_{(z),2,1} = 8}$	
	Layer 2, $\boldsymbol{\lambda_{(z),2,3} = 5}$	
	Layer 3, $\boldsymbol{\lambda_{(z),2,3} = 2}$	
Machine precision deviation $\boldsymbol{\lambda_{(z),3}}$	$\boldsymbol{\lambda_{(z),3} = \pm(0.0001 \times h) = \pm 0.002}$	
Slicing deviation $\boldsymbol{\lambda_{(z),4}}$	Layer 3:$\boldsymbol{\lambda_{(z),4} = H_t - h_{printed} \times E\left(\frac{H_t}{h_{printed}}\right) = 2}$	
Layer 1 vertical deviation on z axis	$\boldsymbol{\lambda_{(z),N1,3} = 8.05}$	
Layer 2 vertical deviation on z axis	$\boldsymbol{\lambda_{(z),N2,3} = 5.05}$	
Layer 3 vertical deviation on z axis	$\boldsymbol{\lambda_{(z),N3,3} = 4.05}$	

** Units: All the used metrics and calculated deviations are in mm

*** The compression deviations are estimated based on previous experimental tests using the same concrete mixture

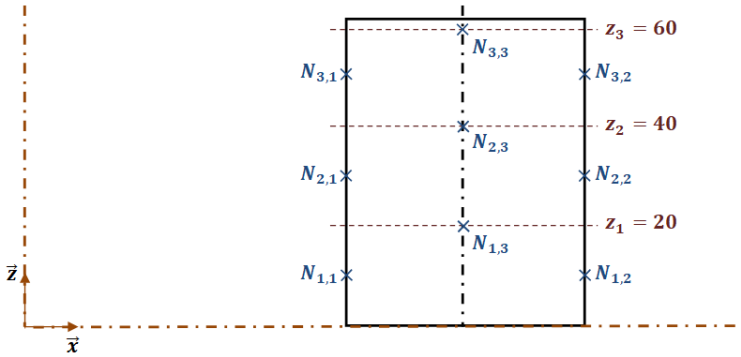

Fig.11. The studied points distribution along the rectangular profile

For lateral deviations, no trowel or smoothing system was used during printing; consequently, the staircase effect remained visible. From previous experimental tests, the radius of the resulting stepped profile was measured as r = 5 mm.

Finally, by incorporating all computed deviations to calculate the printed points ($P_{1.1}$, $P_{1.2}$, $P_{1.3}$, $P_{2.1}$, $P_{2.2}$, $P_{2.3}$, $P_{3.1}$, $P_{3.2}$, $P_{3.3}$) coordinates, the estimated as-printed geometry of the three layers was constructed as depicted in Fig. 12 (To simplify the mathematical formulation, the x-z coordinate system was repositioned so that its origin coincides with the central axis of the rectangular cross-section).

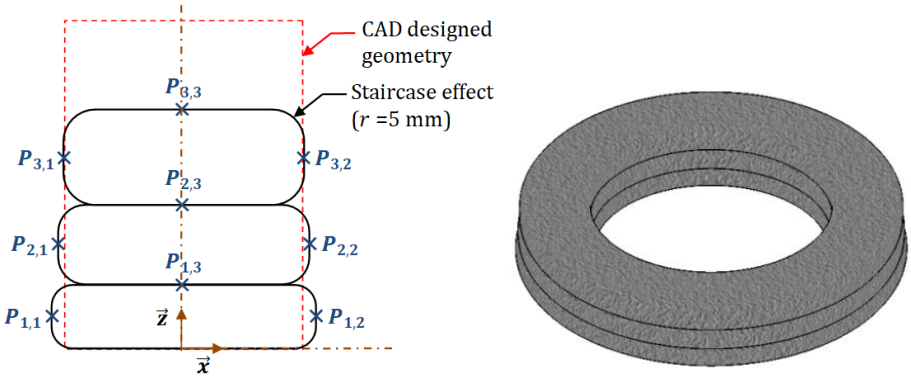

Fig.12. The three layers predicted form and the generated circular wall representation on CATIA V5

5.5.3. COMPARISON ANDANALYSIS

To evaluate the performance of the predictive geometric model, we compare the calculated coordinates of selected points on the circular wall with those measured on the printed specimen. Figure 13 illustrates the printed circular wall at two different stages: (a) one hour after printing and (b) after 28 days of curing.

Two notable observations arise from the inspection of the printed specimen. First, an accumulation of excess material is observed at the transition points between successive layers. This defect is associated with continuous extrusion during non-printing movements and can be mitigated by refining the trajectory code or momentarily interrupting the flow at the end of each layer.

a)

b)

Fig.13. (a) The printed circular wall after 1 hour and (b) after 28 days

Second, the lateral surface exhibits a relatively harsh, non-smooth profile, which suggests an imbalance between the printing speed and the material flow rate. Improving the surface regularity would therefore require reducing the travel velocity or lowering the extrusion rate to allow more uniform material deposition.

Since the extrusion flow rate remained constant, the layer width was relatively uniform around the printed wall. Table 4 presents the coordinates of the nine selected points, comparing the predicted geometry with the experimentally measured values. For the predictive computation of vertical coordinates, the vertical deviation accumulated from the previous layer was added starting from the second layer.

Table 4. Predicted and measured coordinates of the nine studied points

Point	Predicted coordinates		Experimental data	
	x_P	z_P	x_{ex}	z_{ex}
$P_{1.1}$	24.8875	5.975	24.92	5.988
$P_{1.2}$	-24.8875	5.975	-24.92	5.988
$P_{1.3}$	0	11.95	0	11.976
$P_{2.1}$	23.8875	19.425	23.81	19.48
$P_{2.2}$	-23.8875	19.425	-23.81	19.48
$P_{2.3}$	0	26.9	0	26.98
$P_{3.1}$	22.6375	35.875	22.6	35.95
$P_{3.2}$	-22.6375	35.875	-22.6	35.95
$P_{3.3}$	0	44.85	0	44.94

The comparison between the predicted geometry and the experimental measurements shows a high level of alignment, with only minor deviations observed across the selected points. This indicates that the proposed predictive approach is able to reproduce the main geometric trends of the printed structure and can therefore be applied efficiently in practical printing scenarios.

Based on the results analysis, to reduce the deviations on the printed layers we can to adjust several printing parameters, such as reducing the initial layer width to compensate for compression, lowering the printing speed to improve material stability, or using setting accelerators to reduce deformation during layer buildup.

6. DISCUSSION

6.1. MAIN FINDINGS FROM DEVIATION CLASSIFICATION

The deviation classification developed in this study offers a systematic mapping of the main sources of geometric inaccuracy in 3DCP. By segmenting deviations into planar**,** lateral**,** and vertical categories, each linked to specific process, material, environmental, or machine-related parameters, we established a foundation for quantitative prediction of as-built forms. This classification not only clarifies the origin of imprecisions ranging from STL conversion to shrinkage-induced deformation but also provides the basis for targeted mitigation strategies.

6.2. PREDICTIVE FRAMEWORK AND ITS ROLE IN PARAMETER OPTIMIZATION

A predictive modeling framework was put forth to rebuild the actual as-printed shape using input design coordinates and known deviation models, building on the classification findings. The principal aiming is to enable pre-print parameter optimization, which enables users to modify printing parameters beforehand to reduce significant variations. This helps 3DCP reach its long-term objective of closed-loop predictive control.

6.3. TECHNICAL SOLUTIONS TO MITIGATE IMPRECISIONS

For addressing imprecisions in 3DCP, a number of technical strategies might be used:

STL Conversion and Slicing: One of the earliest sources of deviation in 3DCP is the conversion of CAD models to STL and subsequent slicing. Adaptive slicing methods and higher STL mesh resolutions can mitigate staircase effects and polygonal approximation errors. Adaptive MATLAB algorithms for variable nozzle diameters [38], along with geometry-based differentiation between fine and bulk features, have been shown to improve surface accuracy [1]. New slicing strategies, such as non-parallel slicing for complex curved forms [24] and pre-print simulation in Simplify3D [7], as well as voxel-based numerical simulation plugins for Grasshopper [45], are actively being developed.

Nozzle and Extrusion System Improvements: The nozzle output size and geometry directly influence resolution. Smaller diameters enhance precision but slow down build speed. Automated variable nozzle systems [1, 36, 38] allow dynamic adjustments, while mechanical trowels and surface-smoothing tools [8, 44] can reshape layers in real time, reducing bulging and layer misalignment.

Shrinkage phenomenon: Shrinkage effects can be reduced through optimized concrete compositions incorporating mineral additives, fibers, admixtures, or special aggregates [29–31, 46], as well as novel curing methods [31]. Innovative approaches include on-demand activator injectionat the nozzle [47] and **steam curing** for early strength development [48].

Compression and Buildability Enhancement: Compression-related deformations are addressed by reinforcing mixes with steel, glass, carbon, or polymer fibers [1, 5], as well as through numerical modeling to pre-compensate for settlement [1, 34]. Techniques like set-on-demand hardening[49] enable greater buildability by controlling material setting time dynamically.

Post-Processing for Precision: For high-precision applications, CNC milling [50, 51] and laser-based surface correction [52] techniques can be used to remove residual defects and polish external surfaces to final tolerances.

7. CONCLUSION

Ensuring accurate reproduction of the designed geometries remains one of the most persistent challenges in 3DCP. By systematically classifying geometric and dimensional deviations into planar, lateral, and vertical categories, and by relating each type to specific material, process, environmental, and machine parameters, this paper establishes a comprehensive understanding of how inaccuracies originate and propagate during the printing process. Building on this foundation, a predictive modeling framework was developed to integrate CAD-based virtual geometries with mathematically formulated deviation models, enabling the reconstruction of the expected as-printed form with point-wise precision. This approach transforms accuracy control from a predominantly reactive assessment into a proactive predictive tool, capable of informing parameter adjustments before fabrication begins.

The framework’s computational flexibility allows its deployment in research environments such as MATLAB or Python while remaining adaptable for simplified, field-oriented applications in industrial practice. In parallel, the study synthesizes a set of corrective strategies including adaptive slicing, variable-nozzle systems and targeted post-processing, that complement the predictive model and collectively address the major sources of imprecision identified.

A structured methodology for enhancing dimensional accuracy in 3DCP was established by coupling deviation classification with predictive geometry reconstruction and actionable corrective interventions. The integration of computational forecasting with optimized process control offers a viable pathway toward reducing geometric tolerances, improving structural reliability, and advancing the readiness of 3DCP for large-scale, high-precision construction.

FUNDING SOURCES

The authors gratefully acknowledge the support of Sidi Mohamed Ben Abdellah University (USMBA) for covering the publication charges associated with this article.

ACKNOWLEDGEMENT

This research was financially supported by the Institute for Research in Solar Energy and New Energies (IRESEN), which funded the project which this work is included.

REFERENCES

[1] KHAN M.S., SANCHEZ F., ZHOU H., 2020, *3-D Printing of Concrete: Beyond Horizons*, Cement and Concrete Research, 133, 106070, https://doi.org/10.1016/j.cemconres.2020.106070.
[2] NEMATOLLAHIA B., XIAB M., SANJAYAN J., 2017, *Current Progress of 3D Concrete Printing Technologies*, In the 34th International Symposium on Automation and Robotics in Construction, ISARC 2017, 34, 260–267, https://doi.org/10.22260/ISARC2017/0035.
[3] BOS F., WOLFS R., AHMED Z., SALET T., 2016, *Additive Manufacturing of Concrete in Construction: Potentials and Challenges of 3D Concrete Printing*,*Virtual and physical prototyping*,11/3,209–225, https://doi.org/10.1080/17452759.2016.1209867.
[4] LIM S., BUSWELL R.A., LE T.T., AUSTIN S.A., GIBB A.G., THORPE T., 2012, *Developments in Construction-Scale Additive Manufacturing Processes*,*Automation in construction*,21,262–268, https://doi.org/10.1016/j.autcon.2011.06.010.
[5] CHEN Y., HE S., GAN Y., ÇOPUROGLU O., VEER F., SCHLANGEN E., 2022,*A Review of Printing Strategies, Sustainable Cementitious Materials and Characterization Methods in the Context of Extrusion-Based 3D Concrete Printing*, Journal of Building Engineering, 45, 103599, https://doi.org/10.1016/j.jobe.2021.103599.
[6] TAY Y., LI W.D., M.Y., TAN M.J., 2019, *Effect of Printing Parameters in 3D Concrete Printing: Printing Region and Support Structures*, Journal of Materials Processing Technology,271, 261–270, https://doi.org/10.1016/j.jmatprotec.2019.04.007.
[7] XU J., BUSWELL R.A., KINNELL P., BIRO I., HODGSON J., KONSTANTINIDIS N., DING L., 2020,*Inspecting Manufacturing Precision of 3D Printed Concrete Parts Based on Geometric Dimensioning and Tolerancing*, Automation in Construction,117, 103233,https://doi.org/10.1016/j.autcon.2020.103233.
[8] NAIR S.A., SANT G., NEITHALATH N., 2022, *Mathematical Morphology-Based Point Cloud Analysis Techniques for Geometry Assessment of 3D Printed Concrete Elements*, Additive Manufacturing, 49, 102499, https://doi.org/10.1016/j.addma.2021.102499.
[9] LIU X., WANG N., ZHANG Y., MA G., 2024,*Optimization Of Printing Precision And Mechanical Property for Powder-Based 3D Printed Magnesium Phosphate Cement Using Fly Ash*,Cement and Concrete Composites,148, 105482, https://doi.org/10.1016/j.cemconcomp.2024.105482.
[10] SILVA J.M., WAGNER G., SILVA R., MORAIS A., RIBEIRO J., MOULD S., FIGUEIREDO B., NOBREGA J.M., CRUZ P.J.S., 2024, *Real-Time Precision in 3D Concrete Printing: Controlling Layer Morphology Via Machine Vision and Learning Algorithms*, Inventions,9/4, 80,https://doi.org/10.3390/inventions9040080.
[11] MAWAS K., MABOUDI M., GERKE M., 2025,*A Review on Geometry and Surface Inspection in 3D Concrete Printing*,arXivpreprintarXiv,2503,07472, https://doi.org/10.48550/arXiv.2503.07472.
[12] JHUN J., LEE D.-H., UR REHMAN A., KANG S., KIM J.-H., 2024, *Development of a Real-Time Geometric Quality Monitoring System for Extruded Filaments of 3D Concrete Printing Construction*, IEEE Access, 12, 69981–69999, https://doi.org/10.1109/ACCESS.2024.3401472.
[13] CHERIET F., HANI M., LADJAL H.A.E., AZIZ B., 2024, *A Numerical Simulation of Slope Stability with Nailing and Shotcreting Techniques on Natural Ground*, Modeling Earth Systems and Environment,10/4, 5399–5407, https://doi.org/10.1007/s40808-024-02069-1.
[14] ASTM F42, 2015,*Standard Terminology for Additive Manufacturing Technologies*, West Conshohocken: ASTM International.
[15] XU J., DING L., CAI L., ZHANG L., LUO H., QIN W.,2019, *Volume-Forming 3D Concrete Printing Using a Variable-Size Square Nozzle*, Automation in Construction,104, 95–106,https://doi.org/10.1016/j.autcon.2019.03.008.
[16] POLYCHRONOPOULOS N.D., SARRIS I.E., VLACHOPOULOS J.,2024, *Flow Analysis of Screw Extrusion in Three-Dimensional Concrete Printing*, Physics of Fluids, 36/2, https://doi.org/10.1063/5.0193235.
[17] XIA M., NEMATOLLAHI B., SANJAYAN J., 2019,*Printability, Accuracy and Strength of Geopolymer Made Using Powder-Based 3D Printing for Construction Applications*, Automation in Construction, 101,179–189, https://doi.org/10.1016/j.autcon.2019.01.013.

[18] SINGH R., GEHLOT A., AKRAM S.V., GUPTA L.R., JENA M.K., PRAKASH C., SINGH S., KUMAR R., 2021, *Cloud Manufacturing, Internet of Things-Assisted Manufacturing and 3D Printing Technology: Reliable Tools for Sustainable Construction*, Sustainability,13, 7327, https://doi.org/10.3390/su13137327.
[19] MARAIS H., CHRISTEN H., CHO S., DE VILLIERS W., VAN ZIJL G., 2021,*Computational Assessment of Thermal Performance of 3D Printed Concrete Wall Structures with Cavities*,Journal of Building Engineering, 41, 102431, https://doi.org/10.1016/j.jobe.2021.102431.
[20] KLOFT H., EMPELMANN M., HACK N., HERRMANN E., LOWKE D., 2020,*Reinforcement Strategies for 3D-Concrete-Printing*, Civil Engineering Design2/4, 131–139, https://doi.org/10.1002/cend.202000022.
[21] ZHANG Z., 2024,*Common Problems in File Conversion and Processing Parameters of FDM 3D Printer*, Applied and Computational Engineering, 31, 52–56,https://doi.org/10.54254/2755-2721/31/20230121.
[22] MONTALTI A., FERRETTI P., SANTI G.M., 2024,*From CAD to G-Code: Strategies to Minimizing Errors in 3D Printing Process*, CIRP Journal of Manufacturing Science and Technology,55,62–70, https://doi.org/10.1016/j.cirpj.2024.09.005.
[23] EL-QEMARY A., KABBOURI I., BOUTAHARI S., CHAHBOUNI M., 2025,*Anticipation and Correction of Additive Manufacturing Geometric Defects at The Design Stage*, Journal of Machine Engineering, 25/2,74–88, https://doi.org/10.36897/jme/204662.
[24] ZHI Y., TENG T., AKBARZADEH M., 2024, *Designing 3d-Printed Concrete Structures with Scaled Fabrication Models*, ARIN, 3, 28, https://doi.org/10.1007/s44223-024-00070-3.
[25] TRAN N.P., GUNASEKARA C., LAW D.W., HOUSHYAR S., SETUNGE S., CWIRZEN A., 2021,*A Critical Review on Drying Shrinkage Mitigation Strategies in Cement-Based Materials*, Journal of Building Engineering, 38, 102210,https://doi.org/10.1016/j.jobe.2021.102210.
[26] MOELICH G. M., KRUGER J., COMBRINCK R., 2020 *Plastic Shrinkage Cracking in 3D Printed Concrete*, Composites Part B: Engineering, 200,108313, https://doi.org/10.1016/j.compositesb.2020.108313.
[27] GUEHLOUZ I., BELKADI A.A., SOUALHI H., 2025, *Experimental Analysis of Mechanical Behavior, Rheology, and Endogenous Shrinkage in High-Performance Concrete with Flax and Polypropylene Fibers*, Construction and Building Materials, 460, 139856, https://doi.org/10.1016/j.conbuildmat.2025.139856.
[28] LIU J., TIAN Q., WANG Y., LI H., XU W., 2021, *Evaluation Method and Mitigation Strategies for Shrinkage Cracking of Modern Concrete*,Engineering 7/3, 348–357, https://doi.org/10.1016/j.eng.2021.01.006.
[29] ZHU L., ZHANG M., ZHANG Y., YAO J., YANG G., GUAN X., ZHAO Y.,2023, *Research Progress on Shrinkage Properties of Extruded 3D Printed Cement-Based Materials*,Journal of Building Engineering, 77,107394,https://doi.org/10.1016/j.jobe.2023.107394.
[30] RAHUL A.V., MOHAN M.K., DE SCHUTTER G., VAN TITTELBOOM K., 2022, *3D Printable Concrete with Natural and Recycled Coarse Aggregates: Rheological, Mechanical and Shrinkage Behaviour*. Cement and Concrete Composites,125, 104311, https://doi.org/10.1016/j.cemconcomp.2021.104311.
[31] FEDEROWICZ K., KASZYNSKA M., ZIELINSKI A., HOFFMANN M., 2020, *Effect of Curing Methods on Shrinkage Development in 3D-Printed Concrete*, Materials,13/11, 2590, https://doi.org/10.3390/ma13112590.
[32] JAYATHILAKAGE R., RAJEEV P., SANJAYAN J.G., 2020,*Yield Stress Criteria to Assess the Buildability of 3D Concrete Printing.Construction and Building*,Materials, 240,117989, https://doi.org/10.1016/j.conbuildmat.2019.117989.
[33] LIU Z., LI M., QUAH T.K.N., WONG T.N., TAN M.J.,2023, *Comprehensive Investigations on the Relationship Between the 3D Concrete Printing Failure Criterion and Properties of Fresh-State Cementitious Materials*. Additive Manufacturing, 76, 103787, https://doi.org/10.1016/j.addma.2023.103787.
[34] KHAN S.A., İLCAN H., AMINIPOUR E., ŞAHIN O., AL RASHID A., ŞAHMARAN M., KOC M., 2019, *Buildability Analysis on Effect of Structural Design in 3D Concrete Printing (3DCP): An Experimental and Numerical Study*, Case Studies in Construction Materials, 19, e02295, https://doi.org/10.1016/j.cscm.2023.e02295.
[35] ZHANG N., SANJAYAN J., 2023, *Extrusion Nozzle Design and Print Parameter Selections for 3D Concrete Printing*, Cement and Concrete Composites,137, 104939, https://doi.org/10.1016/j.cemconcomp.2023.104939.
[36] DAVID M., FREUND N., DRÖDER K., ET AL., 2023,*The Effects of Nozzle Diameter and Length on the Resulting Strand Properties for Shotcrete 3D Printing*, Materials and Structures,56,157, https://doi.org/10.1617/s11527-023-02246-1.
[37] HUANG X., YANG W., SONG F., ZOU J., 2022,*Study on the Mechanical Properties of 3D Printing Concrete Layers and the Mechanism of Influence of Printing Parameters*, Construction and Building Materials, 335, 127496, https://doi.org/10.1016/j.conbuildmat.2022.127496.
[38] WENXIN L., MINGYANG L., TEGOEH T., 2021, *Variable-Geometry Nozzle for Surface Quality Enhancement in 3D Concrete Printing*, Additive Manufacturing, 37, 101638,https://doi.org/10.1016/j.addma.2020.101638.
[39] MUNTEANU A., CHITARIU D.-F., HORODINCA M., DUMITRAS C.-G., NEGOESCU F., SAVIN A., CHIFAN F., 2021,*A Study on the Errors of 2D Circular Trajectories Generated on A 3D Printer*, Appl. Sci., 11, 11695, https://doi.org/10.3390/app112411695.

[40] KE-TING S.H.I.N., DONG-SHENG A.N., JI-WEI X.I.E., JI-LIN Z.H.O.U., 2024, *Orbital Eccentricity of Celestial Motion–from Stars to Planets*,Chinese Astronomy and Astrophysics, 48/1, 1–40, https://doi.org/10.1016/j.chinastron.2024.03.006.
[41] KABBOURI I., ANASS E.L., CHAHBOUNI M., BOUTAHARI S., 2025,*Modelling Geometric Deviations in Additive Manufacturing of a Cylindrical Surface*, Journal of Machine Engineering,25,https://doi.org/10.36897/jme/211736.
[42] MAROSZEK M., RUDZIEWICZ M., HUTYRA A., DZIURA P., HEBDA M., 2024,*Evaluation of 3D Concrete Printing Extrusion Efficiency*, Appl. Sci., 14, 11866, https://doi.org/10.3390/app142411866.
[43] YUAN P.F., ZHAN Q., WU H., BEH H.S., ZHANG L., 2022,*Real-Time Toolpath Planning and Extrusion Control (RTPEC) Method for Variable-Width 3D Concrete Printing*, Journal of Building Engineering, 46,103716, https://doi.org/10.1016/j.jobe.2021.103716.
[44] HE L., PAN J., HEE Y.S., CHEN H., LI L.G., PANDA B., CHOW W.T., 2024,*Development of Novel Concave and Convex Trowels for Higher Interlayer Strength of 3D Printed Cement Paste*, Case Studies in Construction Materials, 21, e03745,https://doi.org/10.1016/j.cscm.2024.e03745.
[45] VANTYGHEM G., OOMS T., DE CORTE W., 2021, *Voxelprint: A Grasshopper Plug-In for Voxel-Based Numerical Simulation of Concrete Printing*,Automation in Construction, 122,103469, https://doi.org/10.1016/j.autcon.2020.103469.
[46] TRAN M.V., CU Y.T., LE C.V., 2021, *Rheology and Shrinkage of Concrete Using Polypropylene Fiber for 3D Concrete Printing*, Journal of Building Engineering, 44, 103400, https://doi.org/10.1016/j.jobe.2021.103400.
[47] MUTHUKRISHNAN S., RAMAKRISHNAN S., SANJAYAN J., 2022,*Set on Demand Geopolymer Using Print Head Mixing for 3D Concrete Printing*,Cement and Concrete Composites, 128, 104451,https://doi.org/10.1016/j.cemconcomp.2022.104451.
[48] WANG B., YAO X., YANG M., ZHANG R., HUANG J., WANG X., DONG Z., ZHAO H., 2022,*Mechanical Performance of 3D Printed Concrete in Steam Curing Conditions*, Materials,15, 2864,https://doi.org/10.3390/ma15082864.
[49] MUTHUKRISHNAN S., RAMAKRISHNAN S., SANJAYAN J., 2021,*Technologies for Improving Buildability in 3D Concrete Printing*, Cement and Concrete Composites, 122, 104144, https://doi.org/10.1016/j.cemconcomp.2021.104144.
[50] BUSWELL R., XU J., DE BECKER D., DOBRZANSKI J., PROVIS J., KOLAWOLE J.T., KINNELL P.. 2022,*Geometric Quality Assurance for 3D Concrete Printing and Hybrid Construction Manufacturing Using a Standardised Test Part for Benchmarking Capability*,Cement and Concrete Research, 156, 106773, https://doi.org/10.1016/j.cemconres.2022.106773.
[51] DOBRZANSKI J., BUSWELL R., CAVALARO S., KINNELL P., WANG W., XU J., KOLAWOLE J., 2022,*Milling a Cement-Based 3D Printable Mortar in Its Green State Using a Ball-Nosed Cutter*, Cement and Concrete Composites, 125, 104266, https://doi.org/10.1016/j.cemconcomp.2021.104266.
[52] MUSHTAQ R.T., WANG Y., KHAN A.M., REHMAN M., LI X., SHARMA S., 2023,*A Post-Processing Laser Polishing Method to Improve Process Performance of 3D Printed New Industrial Nylon-6 Polymer*, Journal of Manufacturing Processes, 101, 546–560, https://doi.org/10.1016/j.jmapro.2023.06.019.